



Analytical stress-strain model and damage index for confined and unconfined concretes to simulate RC structures under cyclic loading

K. Sadeghi*

Received: February 2013, Revised: October 2013, Accepted: January 2014

Abstract

An analytical nonlinear stress-strain model and a microscopic damage index for confined and unconfined concretes together with a macroscopic damage index for reinforced concrete (RC) structures under cyclic loading are proposed. In order to eliminate the problem of scale effect, an adjustable finite element computer program was generated to simulate RC structures subjected to cyclic loading. By comparing the simulated and experimental results of tests on the full-scale structural members and concrete cylindrical samples, the proposed stress-strain model for confined and unconfined concretes under cyclic loading was accordingly modified and then validated. The proposed model has a strong mathematical structure and can readily be adapted to achieve a higher degree of precision by modifying the relevant coefficients based on more precise tests.

To apply the proposed damage indices at the microscopic and macroscopic levels, respectively, stress-strain data of finite elements (confined and unconfined concrete elements) and moment-curvature data of critical section are employed, respectively. The proposed microscopic damage index can easily be calculated by using the proposed simple analytic nonlinear stress-strain model for confined and unconfined concretes. The proposed macroscopic damage index is based on the evaluation of nonlinear local degradation of materials and taking into account the pseudo-plastic hinge produced in the critical section of the structural element. One of the advantages of the proposed macroscopic damage index is that the moment-curvature data of the critical section is sufficient in itself and there is no need to obtain the force-displacement data of the structural member.

Keywords: Stress-strain model, Confined and unconfined concretes, Damage index, Cyclic loading, Numerical simulation, Reinforced concrete structures.

1. Introduction

Confined concrete can sustain much higher strains without strength degradation compared to unconfined concrete. This enhanced performance can be achieved only when the unconfined cover concrete has failed and spalled. Among several models have been proposed to determine the law governing the behavior of confined compressive concrete confined within rectangular or spiral stirrup ties. Among these, the models of Kent and Park, Vallenias et al., and Sheikh and Uzumeri have been used for the calculation of the theoretical flexural strength of columns. Researchers such as Mander et al., Scott et al., Sheikh and Uzumeri and Vallenias et al. have performed several tests on real full-scale structures.

A complex mathematical model was developed by Bazant and Bhat. Apparently this model is the sole model that considers the stress-strain relation for the monotonic,

cyclic and dynamic loading of confined and unconfined concretes under any state of multi-axial stresses.

However this model has been developed by using mainly the data based on the biaxial and tri-axial tests with the confinement provided by mechanical means.

The proposed model by Kent and Park to describe the behavior of concrete confined within rectangular stirrup ties was based on the experimental tests results of Roy and Sozen and of other researchers who have taken into account the enhancement of ductility strength.

Scott et al. and Park et al. have also worked on the full-scale columns of buildings. By considering the augmentation of concrete's strength due to confinement and the effect of the strain velocity, they proposed modification to the behavior model of Kent and Park.

Vallenias et al., and Sheikh and Uzumeri have proposed the monotonic stress-strain equation for concrete confined by rectangular transverse reinforcements that takes into account the above-mentioned considerations. Park et al., Desayi et al., Ahmad and Shah, Meyer, CEC, Mander, Sheikh et al., Fu et al. and Tassios and others have also proposed equations for the monotonic stress-strain model of concrete confined by spiral or circular transverse reinforcements.

* Corresponding author: ksadeghi@gau.edu.tr
1 Associate Professor, Civil Engineering Department, Girne American University, Girne, North Cyprus, Via Mersin 10, Turkey

The effectiveness of transverse reinforcement in providing confinement depends upon the spacing and arrangement of this steel in the section [1]. The effective section area of confined concrete increases as the spacing of the spiral or ties decreases. Confinement in a RC column can lead to an increase in strength, ultimate strain and as well as in ductility. An important feature of the behavior is the maximum strain that can be sustained by the concrete, as this has a major influence on the ductility. The limiting concrete strain has been found to be reached when one or more of the confining ties fail in tension.

In the following, a model for confined and unconfined concretes under cyclic compression loading is proposed by the author.

Existing damage indices are based on different characteristics such as the number of cycles, stiffness, ductility and energy.

The damage index proposed by Park and Ang [2] which is based on the plastic-hinge approach and consists of both deformation and energy terms, has been criticized by Abbasnia et al. [3] and some other researchers.

In some of the existing energy-based damage indices (proposed by Meyer and Garstka), an additional monotonic loading test is needed for the cyclic loading cases because in these damage indices, absorbed energy to failure of monotonic loading is used as normalizing factor for cyclic loading cases. Therefore some adaptation measures are also required. The distribution of Meyer's damage index "D" between 0% and 100%, especially for repeated cycles, is not valid. This approach has been criticized by the author which confirmed by Garstka and other researchers. In the global energy based damage index proposed by the author [4], a cyclic normalizing factor is used and therefore no adaptation factor is needed and the value of "D" becomes exactly 100% at failure while following a regular distribution. To determine "D", the calculation of displacements for several sections or for the critical section is necessary.

The goal of this paper is to present an analytical nonlinear stress-strain model and a microscopic damage index for confined and unconfined concretes that can be applied to the simulation of concrete finite elements within the sections of RC structures together with a simplified macroscopic damage index for RC structures under cyclic loading. The macroscopic damage index is based on the local degradation of materials for RC structures under any type of cyclic loading by considering moment-curvature data at critical sections (without the calculation of displacements) of the structural member.

2. Experimental Data

The experimental test results carried out by Garcia Gonzalez [5] and Park et al. [6] are mainly used for the global validation of the proposed models. The experimental test results on the confined and unconfined concrete samples performed by the author [7], Lamirault [8], Al Sulayfani [9], Tassios [10], Park [6], Buyukozturk [11], Meyer [12], Darwin [13], Bazant and Kim [14], Sinha et al. [15], Karsan and Jirsa [16] and Mander et al.

[17] are also used for local validation.

Over 20 tests performed by Garcia Gonzalez [5] on full-scale columns under bi-axial alternating cyclic and axial loading were used. The horizontal loads through different horizontal directions of angles Ω with the main axis of cross-section have been applied on the top of the columns. Over 55 cylindrical samples of confined and unconfined concretes were also tested [7].

3. Finite Element Computer Program

A computer program entitled "Structural Analysis and Damage Evaluation Program" (SADEP) has been developed by the author [4] to simulate numerically the behavior of RC structures under cyclic loading.

SADEP has some sub-programs such as BBSC (Biaxial Bending Column Simulation) which is used as Base Model, CCS (Confined Concrete Simulation), UCS (Unconfined Concrete Simulation) and SBS (Steel Bars Simulation).

In BBSC, behavior models for confined and unconfined concretes generated by using CCS and UCS are considered and the behavior models of structural members are specified. After an iterative process the simulated and experimental results are compared and the concrete stress-strain models are adjusted accordingly. The selected models presented here are simple but sufficiently accurate to be used in a cyclic simulation.

In BBSC, each section of structure is discretized into finite elements. For compressive confined and unconfined concrete elements, the cyclic stress-strain models proposed by the author and for reinforcements the expression proposed by Park and Kent [6] based on the Ramberg-Osgood cyclic model have been used. The concrete tensile stress is assumed to be linear up to the concrete tensile strength. The CEB code specification [18] was used for the maximum compressive strain value for unconfined concrete, and the value proposed by Sheikh [19] employed for confined concrete.

The basic equilibrium is justified over a critical hypothetical cross-section assuming the Navier law with an average curvature. The method used qualifies as a "Strain Plane Control Process" that requires the resolution of a quasi-static simultaneous equations system using a triple iteration process over the strains [4]. For this procedure, the strains in the extreme compressive and tensile points of the section are considered as the two main variables. The program takes into account the confining effect of the transverse reinforcement and simulates the loss of the concrete cover. It allows the determination of the failure, the local internal behavior of critical section (i.e. strains, stresses, neutral axis, microscopic damage index, etc.) and the global external behavior of the column (deflection, average rigidity, equivalent viscous damping ratio, macroscopic damage index, etc.). The simulated results obtained using SADEP are in the main confirmed by the full-scale experimental results obtained by other researchers [5, 20, 6].

4. Proposed Stress-Strain Model for Confined and

Unconfined Concretes

4.1. Methodology

In order to eliminate the problem of scale effect, in addition to using the results of tests on concrete samples, SADEP was used and the simulated and experimental test results on the full-scale columns were compared. In this way the proposed non-linear stress-strain model for confined and unconfined concretes under cyclic loading was modified and validated.

The stress-strain curve of unconfined concrete under monotonic loading is used as the envelope curve for the cyclic loading case as confirmed by the author [21, 7], Sinha et al. [15], Karsan and Jirsa [16] and Al Sulayfani [9]. A similar relationship also holds for confined concrete [17]. This confirmed relationship between the cyclic and monotonic loading curves are used in the proposed model.

4.2. Examples of evaluation and modification of the parameters

Utilization of an unconfined model similar to that of Al Sulayfani [9] for the simulation of a RC element's behavior results in more closely spaced hysteresis loops than are obtained by the experimental tests on the columns of Garcia Gonzalez [5]. To further investigate the problem, the models of Park [6], Buyukozturk [11], Meyer [12], Darwin [13], Bazant and Kim [14] and Karsan and Jirsa [16] have been studied. Comparative studies on the parameters relating to the point of unloading (slope at the point of unloading and the coordinates of plastic residual stress) have been performed. By performing numerical simulation on the columns using SADEP and comparing

these results with the experimental test of Garcia Gonzalez [5], it was observed that, the values of unloading tangent modulus E_{U0} and plastic residual strain ε_r (the plastic residual strain is defined as the residual axial strain of concrete when it is unloaded to zero stress[22] (see Fig. 2)) which are used for generating the stress-strain ($\sigma - \varepsilon$) curve play a very significant role in the moment-curvature response of the section of a RC member in the unloading phase. As shown in Fig. 2, the variation of E_U is less important, because its effect is situated in the zone of lesser stresses. The plastic residual strain ε_r has a non-negligible role in the failure phenomenon in the case of cyclic loading. If this strain is considered greater than the actual case, the failure appears sooner in the response curve. Conversely, if a value of ε_r smaller than the actual one is adopted, the number of cycles at failure and the values of the displacement and the curvature will reduce. In Table 1, the variations of the values of $\varepsilon_r/\varepsilon_0$ as a function of $\varepsilon_A/\varepsilon_0$ obtained by using different researchers models are presented (see also Fig. 2).

Comparison of the simulated results by using SADEP and the experimental of Meyer, indicates a close agreement between the proposed $\varepsilon_r/\varepsilon_0$ values and the experimental of Meyer values.

As another example, if the value of E_{U0} is assumed to be smaller than the actual case, the hysteresis loops in the response curve (moment-curvature or force-displacement curves) are more closed. This kind of verification and comparison with the experimental test results is used to determine all the parameters and coefficients of the proposed model. These calculations and verifications are performed by applying SADEP.

Table 1 Values of $\varepsilon_r/\varepsilon_0$ obtained by using different models

$\varepsilon_A/\varepsilon_0$	0.3	0.5	0.7	1.0	1.2	1.5	1.7	2.0
Al Sulayfani's model	0.019	0.042	0.081	0.182	0.289	0.528	0.751	1.199
Meyer's model	0.024	0.068	0.132	0.340	0.442	0.615	0.744	0.960
Karsan's model	0.052	0.101	0.162	0.275	0.365	0.521	0.640	0.840
Buyukozturk's model	0.079	0.165	0.277	0.496	0.675	0.995	1.240	1.660

4.3. Proposed stress-strain model for confined concrete

The following stress-strain model is proposed to simulate numerically the behavior of confined and also unconfined concrete elements discretized within the sections of RC members.

4.3.1. Stress-strain model for confined concrete under monotonic loading

The proposed analytic equation for the stress-strain model of confined concrete under monotonic compression loading is described below. Equation (1) presents a simple mathematical model that is valid for concretes with the strengths within the range of $20 \text{ MPa} < f'_c < 50 \text{ MPa}$. Fig. 1 presents schematically the proposed stress-strain curves

obtained for confined and unconfined concretes under monotonic loading. These curves are also used as the envelope curves for the cyclic loading cases.

$$\sigma = \frac{f'_{cc}}{A_L \left(\frac{\varepsilon}{\varepsilon_{c0}}\right)^2 + B_L \left(\frac{\varepsilon}{\varepsilon_{c0}}\right) + C_L + D_L \left(\frac{\varepsilon}{\varepsilon_{c0}}\right)^{-1}} \quad (1)$$

The relationship between the coordinates of the peaks of confined and unconfined concretes [10, 21] are given as:

$$f'_{cc} = f'_c (1.000 + 2.5a \cdot \omega_w) \quad \text{for} \quad \sigma/f'_c < 0.05 \text{ or } a \cdot \omega_w < 0.1 \quad (2)$$

$$f'_{cc} = f'_c (1.125 + 1.25a \cdot \omega_w) \quad \text{for} \quad \sigma/f'_c \geq 0.05 \text{ or } a \cdot \omega_w \geq 0.1 \quad (3)$$

$$\varepsilon_{c0} = \varepsilon_0 \left(\frac{f'_{cc}}{f'_c} \right)^2 \quad (4)$$

$$\text{With: } \omega_w = k \left(\frac{A_t}{b_{max} \cdot S_t} \right) \left(\frac{f_{yt}}{f'_c} \right) \quad (5)$$

$$a = a_n \cdot a_s \quad (6)$$

$$a_n = 1 - \frac{8}{3\eta} \quad (a_n = 1 \text{ for circular sections}) \quad (7)$$

$$a_s = \left(1 - \frac{S_t}{2b_0} \right)^2 \text{ for rectangular and circular sections} \quad (8)$$

$$a_s = \left(1 - \frac{S_t}{2b_0} \right) \text{ for circular sections with spiral transverse reinforcements} \quad (9)$$

Where, σ represents the stress, ε represents the strain, f'_c and f'_{cc} represent compressive strengths of unconfined

and confined concretes at 28 days, respectively, ε_0 and ε_{c0} represent the strains related to f'_c and f'_{cc} , respectively, A_t represents the cross sectional area of a transverse reinforcement, f_{yt} represents the yield stress of transverse reinforcement, b_{max} represents the larger dimension of the section, S_t represents the longitudinal spacing between transverse reinforcements, a represents the confinement efficiency factor defined as the ratio of the confined area over the total area, a_n represents the transverse reinforcements form factor, a_s represents the transverse reinforcements spacing factor, and b_0 represents the distance between external longitudinal reinforcements in the column section. The factors k and η used in equations (5) and (7) for some forms of transverse reinforcements [21, 10] are given in Table 2.

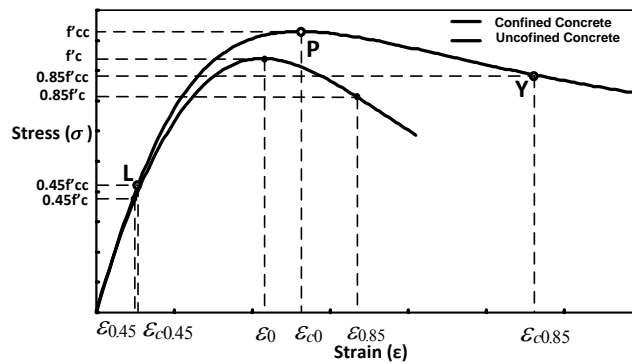


Fig. 1 Proposed stress-strain curves for confined and unconfined concretes under monotonic loading (Envelope curve for cyclic loading cases)

Table 2 Values of k and η for some forms of transverse reinforcements [21, 10]

Form of trans. reinf.	k^*	η
	4	4
	6	8
	6,83	8
	7,22	12
	8	12
	9,33	12
	12,83	16
	10	16
	10,8	16

* $K = 4$ in case of circular transverse reinforcement.

By inserting the relevant values of stress and strain in equation (1) at points L, P and Y and also recognizing that the slope of the curve is equal to zero at the peak of the curve (see Fig. 1), the four unknown coefficients A_L , B_L , C_L and D_L are determined. These four conditions (coordinates of the points L, P and Y and also the slope at point P) are as follows:

- Point L ($\varepsilon_{c0.45}$, $0.45f'_{cc}$) on the confined concrete stress-strain curve:

$$\text{with: } \varepsilon_{c0.45} = (0.45 f'_{cc})/E_{c0.45} \quad (10)$$

$$\text{and secant modulus: } E_{c0.45} = 4861 (f'_{cc})^{0.49} \quad (11)$$

- Point P at maximum stress of confined concrete stress-strain curve at coordinates (ε_{c0} , f'_{cc}):

$$\varepsilon_{c0} = 0.00085 (f'_{cc})^{0.246} \quad (f'_{cc} \text{ in MPa}) \quad (12)$$

$$\sigma_{c0} = f'_{cc} \quad (13)$$

The supplementary condition of zero slope (tangent) at point P gives:

$$\frac{d\sigma}{d\varepsilon} = 0 \quad (14)$$

- Point Y ($\varepsilon_{c0.85}$, $0.85f'_{cc}$) on the confined concrete stress-strain curve:

$$\varepsilon_{c0.85} = \varepsilon_{0.85} + 0.1\omega_w \quad (15)$$

$$\sigma_{c0.85} = 0.85f'_{cc} \quad (16)$$

where: $\varepsilon_{0.85} = (1.9 - 0.008f'_{cc})\varepsilon_0$ (f'_{cc} in MPa) (17)

4.3.2. Stress-strain model for confined concrete under cyclic loading

4.3.2.1. Unloading curve

As shown in Figs. 2 to 4, unloading may occur either from the envelope curve or from a phase of reloading. In both cases, the equation (18) gives the stress-strain curve for unloading.

$$\sigma = [A_U \left(\frac{\varepsilon}{\varepsilon_{c0}}\right)^3 + B_U \left(\frac{\varepsilon}{\varepsilon_{c0}}\right)^2 + C_U \left(\frac{\varepsilon}{\varepsilon_{c0}}\right) + D_U] f'_{cc} \quad (18)$$

The four unknown factors A_U , B_U , C_U and D_U can be found by applying the coordinates and slopes of two extreme points on the unloading curve (i.e. the starting and finishing points on the unloading curve).

a) Unloading from the envelope curve

In the case of unloading from the envelope curve (see Fig. 2), to find the unknown factors A_U , B_U , C_U and D_U , the coordinates and slopes at points $A(\varepsilon_A, \sigma_A)$ and $B(\varepsilon_r, 0)$ are used.

The tangent modulus at point A is given as follows:

$$E_{U0} = 10\sigma_A / [3(\varepsilon_A - \varepsilon_r)] \quad (19)$$

The plastic residual strain ε_r at point B, depending on the unloading starting point coordinates (point A) can be found from the equation (20) or (21).

$$\varepsilon_r = [0.27 \left(\frac{\varepsilon_A}{\varepsilon_{c0}}\right)^2] \varepsilon_{c0} \quad \text{for} \quad \frac{\varepsilon_A}{\varepsilon_{c0}} \leq 1 \quad (20)$$

$$\varepsilon_r = [0.14 \left(\frac{\varepsilon_A}{\varepsilon_{c0}}\right)^2 + 0.2 \frac{\varepsilon_A}{\varepsilon_{c0}}] \varepsilon_{c0} \quad \text{for} \quad \frac{\varepsilon_A}{\varepsilon_{c0}} \geq 1 \quad (21)$$

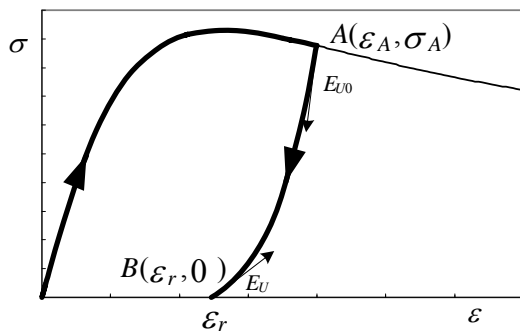


Fig. 2 Unloading from the envelope curve

The tangent modulus at point B can be found from the equation (22) or (23).

$$E_U = \left[\frac{0.72}{0.95 + 6.5 \frac{\varepsilon_r}{\varepsilon_{c0}}} \right] E_{c0.45} \quad \text{for} \quad \frac{\varepsilon_r}{\varepsilon_{c0}} < 1 \quad (22)$$

$$E_U = \left[\frac{\frac{\varepsilon_r}{\varepsilon_{c0}} - 49.99}{48.8} \right] E_{c0.45} \quad \text{for} \quad 1.6 \leq \frac{\varepsilon_r}{\varepsilon_{c0}} < 5 \quad (23)$$

b) Unloading from a phase of reloading

In the case of unloading from a phase of reloading, depending on the coordinates of unloading point (C or D) comparing with the coordinates of point A (ε_A, σ_A), different moduli are used as given below and as shown in Figs. 3 and 4.

b1) Unloading from a point C where $\varepsilon_C < \varepsilon_A$

- Point C (ε_C, σ_C):

The coordinates of point A have been determined in the previous step.

The value of unloading tangent modulus (E_{UC}) at point C is obtained by linear interpolation between the modulus E_{U0} at point A and E_U at point B which is given in equation (24).

$$E_{UC} = E_{U0} - \frac{(E_{U0} - E_U)}{(\varepsilon_A - \varepsilon_r)} \quad (24)$$

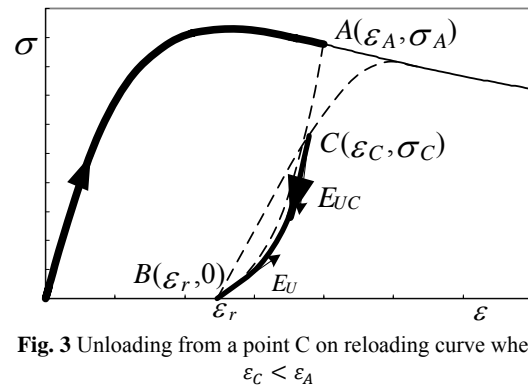


Fig. 3 Unloading from a point C on reloading curve when $\varepsilon_C < \varepsilon_A$

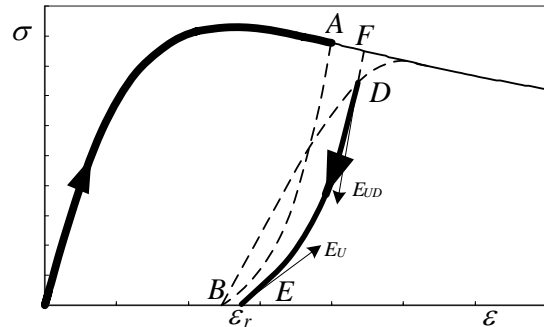


Fig. 4 Unloading from a point D on the reloading curve when $\varepsilon_D > \varepsilon_A$

- Point B ($\varepsilon_r, 0$):

The coordinates of point B have been determined in the previous step by applying the equation (20) or (21). The value of tangent modulus E_U at point B has also been calculated by using the equation (22) or (23).

b2) Unloading from a point D where $\varepsilon_D > \varepsilon_A$

For the trajectory shown in Fig. 4, the two points D and E that the curve DE passes through them are determined as follows:

- Point D (ε_D, σ_D):

The coordinates of point D have been determined in the previous step.

The value of the unloading tangent modulus (E_{UD}) at point D is obtained by linear interpolation between the modulus E_{U0} at point F and E_U at point E. The point F is

defined as the intersection of the line of slope $1.5E_{c0.45}$ passing from point D with the envelope curve. By applying the coordinates of point F instead of the coordinates of point A, equation (19) allows the determination of the unloading modulus at point F. E_{UD} can then be found by using equation (25):

$$E_{UD} = E_{U0} - \frac{(E_{U0} - E_U)}{(\varepsilon_F - \varepsilon_r)} \quad (25)$$

- Point E ($\varepsilon_r, 0$):

The coordinates of point E are determined by applying ε_r instead of ε_A in equation (20) or (21).

The value of tangent modulus E_U at point E is calculated by applying ε_r of point E in the equation (22) or (23).

4.3.2.2. Reloading curve

Equation (26) is used for the reloading curve:

$$\sigma = [A_R \left(\frac{\varepsilon}{\varepsilon_{c0}}\right)^3 + B_R \left(\frac{\varepsilon}{\varepsilon_{c0}}\right)^2 + C_R \left(\frac{\varepsilon}{\varepsilon_{c0}}\right) + D_R] E_{c0.45} \quad (26)$$

The four unknown factors A_R , B_R , C_R and D_R are found by applying the coordinates and slopes of the two extreme points of the reloading curve (i.e. the starting point of reloading phase and the extreme point on the envelope curve).

As shown in Figs. 5 and 6, reloading from zero stress and reloading from an unloading trajectory are considered in two different cases as follows:

- Reloading from a zero stress status (plastic residual strain)

For the trajectory BG shown in Fig. 5, the two points B and G that the curve BG passes through them are determined as follows:

- Point B ($\varepsilon_r, 0$):

The coordinates of point B have been determined in the previous steps.

The value of reloading tangent modulus E_R at point B can be obtained from equation (27):

$$E_R = \left[\frac{1}{0.95 + 2.78 \frac{\varepsilon_r}{\varepsilon_{c0}}} \right] E_{c0.45} \quad (27)$$

- Point G (ε_G, σ_G):

$$\varepsilon_G = 1.22\varepsilon_A \quad (28)$$

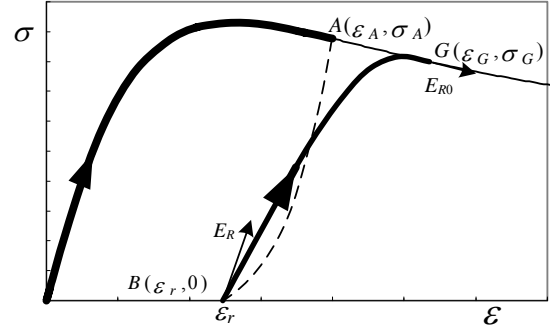


Fig. 5 Reloading from a point of zero stress

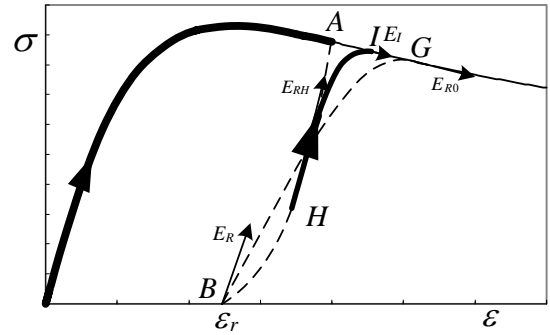


Fig. 6 Reloading from a point on the unloading trajectory

The modulus E_{R0} is the tangent modulus on the envelope curve at point G.

- Reloading from an unloading trajectory

For the trajectory HI shown in Fig. 6, the coordinates and slopes of the two points H and I at the starting and finishing points of the curve HI are determined as follows:

- Point H (ε_H, σ_H):

The coordinates of point H have been determined in the previous step.

The tangent modulus E_{RH} at point H is considered to be equal to E_R and can be calculated by using equation (27).

- Point I (ε_I, σ_I):

The strain at point I is calculated by using equation (29).

$$\varepsilon_I = \left[(K\varepsilon_A - \varepsilon_r) + (1 - K)\varepsilon_H \right] \frac{\varepsilon_A}{\varepsilon_A - \varepsilon_r} \quad (29)$$

where: $K = 1.22$

The strain at point I, found from equation (29), gives $\varepsilon_I = \varepsilon_A$ when $\varepsilon_H = \varepsilon_A$ and gives $\varepsilon_I = \varepsilon_G = K\varepsilon_A$ (see equation (28)) when $\varepsilon_H = \varepsilon_r$ (i.e. the point H is positioned on the point B).

The stress σ_I and modulus E_I at point I can be found by using its strain and the envelope curve.

4.4. Proposed stress-strain model for unconfined concrete

By replacing suffixes cc, c0, c0.45, c0.85 with c, 0, 0.45, 0.85, respectively in equations (1), (10) to (14) and (16) to (29) the stress-strain model for unconfined concrete is found.

4.5. Application of the proposed model

Two examples of the application of the proposed stress-strain model for confined and unconfined concretes under monotonic and cyclic loading are shown in Figs. 7 and 8.

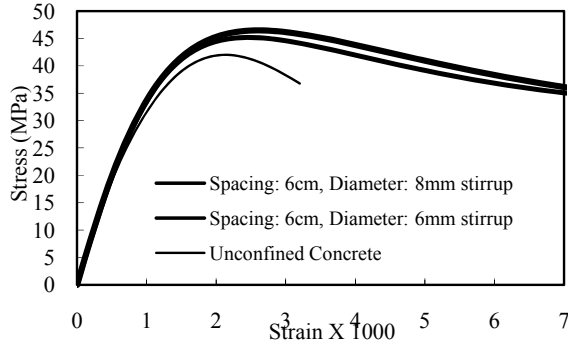


Fig. 7 Effect of the spacing of transverse reinforcements, $f'_c = 42$ MPa

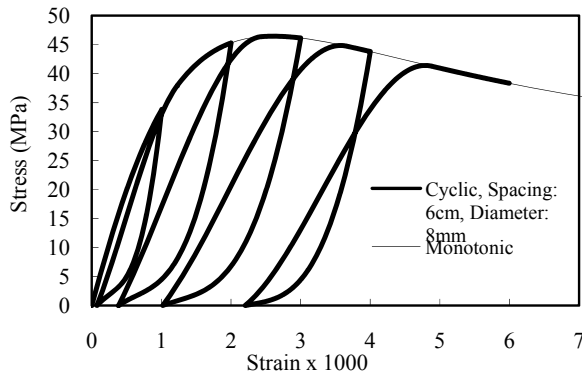


Fig. 8 An example of the application of the proposed stress-strain model, $f'_c = 42$ MPa

Fig. 7 shows an example for the application of the proposed model for unconfined concrete and confined concrete with transverse reinforcements (having 6 cm spacing and diameters of 8 mm and 6 mm).

It can be seen from Fig. 7 that the presence of the transverse reinforcements significantly increases the strength of the RC element and this influence is very significant after achieving the maximum strength (after peak point).

Fig. 8 shows another example of the application of the proposed stress-strain model to confined concrete (concrete of strength $f'_c = 42$ MPa confined within rectangular stirrup ties of diameter 8 mm and a longitudinal spacing of 6 cm) under monotonic and cyclic loading.

4.6. Validation of the proposed stress-strain model

In this section, some examples of comparison of simulated results using the proposed stress-strain model and experimental test results of full-scale RC members are presented.

The proposed stress-strain simulation for confined

concrete and Mander's simulation and experimental test results [23] are compared in Fig. 9. As this figure shows, the strain at peak about 6‰ is overestimated by Mander, while this strain and the rate of reduction of stress after the peak in the proposed model fits better with the results of other researchers (e.g.: Belmouden and Lestuzzi [24] reported strain at peak of about 0.00267 for confined concrete of strength $f'_c = 48$ MPa).

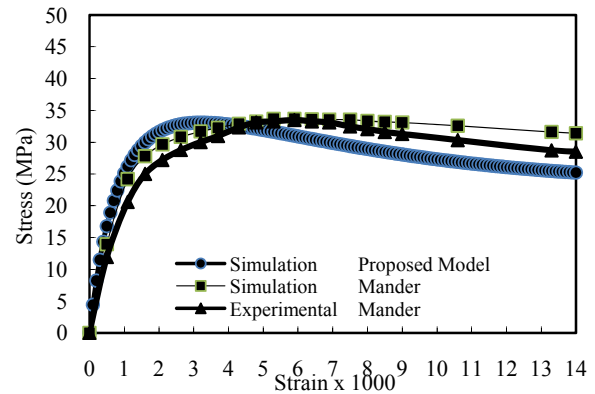


Fig. 9 Comparison of the proposed model with experimental tests and simulation of Mander [23]

Comparison of numerically simulated results obtained for RC members using the proposed stress-strain model and experimental tests on full-scale members are reflected in Fig.10 to Fig. 14.

In Figures 10 and 11 the simulated results using the proposed model and experimental tests of Garcia Gonzalez [5] on columns under monotonic lateral oriented loads of angles $\Omega = 0^\circ$ and $\Omega = 45^\circ$ with axial load are compared.

Fig. 12 shows the comparison between the simulated results using the proposed model and the experimental and simulated results of Park et al. [6] on RC members under alternating mono-axial bending moment.

In Figs. 13 and 14, the average rigidity and equivalent viscous damping ratio when applying the proposed model and experimental tests [5] for cyclic loading are compared.

Comparison of the simulated and experimental test results indicates a close agreement between simulations using the proposed model and the experimental tests on full-scale RC members.

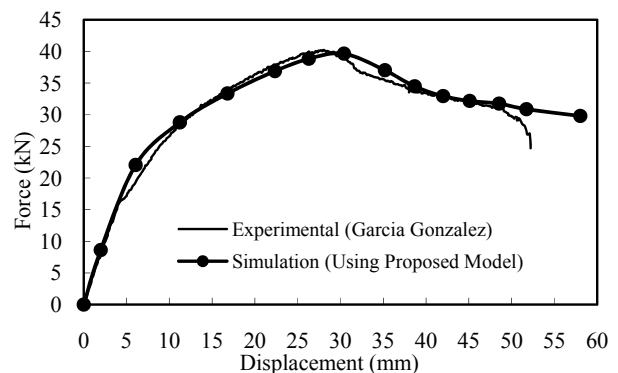


Fig. 10 Comparison of simulated results using the proposed model and experimental tests of Garcia Gonzalez [5], $\Omega = 0^\circ$

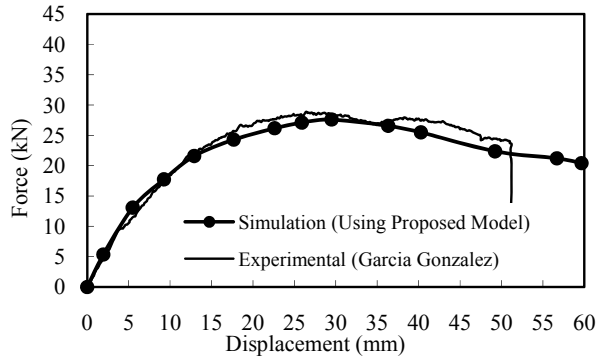


Fig. 11 Comparison of simulated results using the proposed model and experimental tests of Garcia Gonzalez [5], $\Omega = 45^\circ$

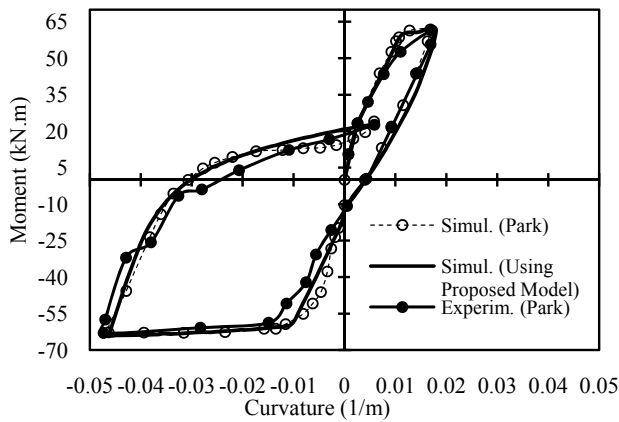


Fig. 12 Comparison of simulated results using the proposed model and experimental tests and simulation of Park [6]

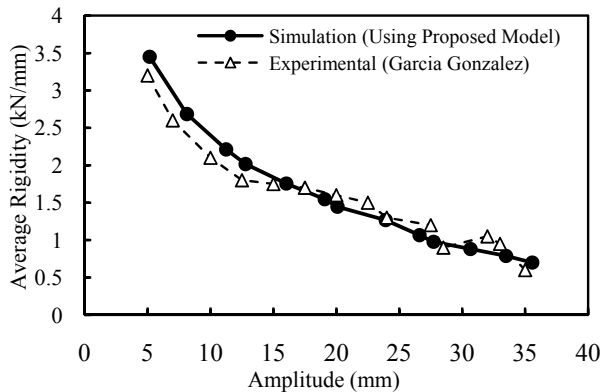


Fig. 13 Comparison of the average rigidity when using the proposed model and experimental tests [5], cyclic loading, $\Omega = 30^\circ$

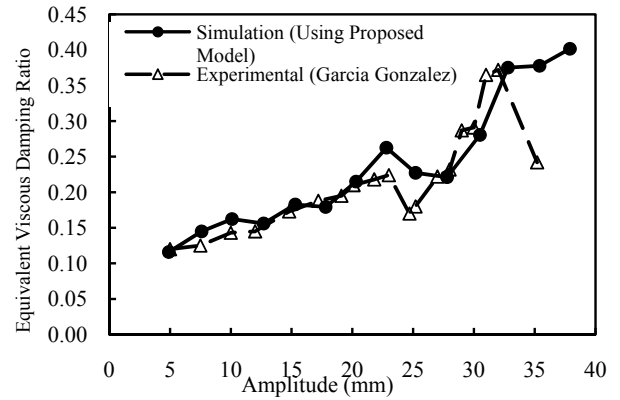


Fig. 14 Comparison of equivalent viscous damping ratio when using the proposed model and experimental tests [5], cyclic loading, $\Omega = 30^\circ$

5. Damage Index

Both a damage index applicable to confined and unconfined concretes elements (microscopic level) and a damage index (derived from energy-based damage index [4]) for sections of RC structural members (macroscopic level) subjected to cyclic and monotonic loading are proposed in this paper.

5.1. "Primary half-cycle" and "following half-cycle" concepts

Following Otes [25] a "primary half-cycle (PHC)" is considered when any half-cycle reaches a new maximum displacement: it is followed by a certain number of "following half-cycles (FHC)" with smaller displacements. Whenever a certain maximum displacement, corresponding to the primary half-cycle (PHC)_i is exceeded, a new primary half-cycle (PHC)_{i+1} is established. Every PHC corresponds to a certain damage degree.

5.2. Proposition of a Microscopic damage index for Concrete

A microscopic damage index (D) for confined and unconfined concretes is proposed as represented by the equation (30).

$$D = \frac{\sum_{i=1}^n \int_{\epsilon_{p(i-1)}}^{\epsilon_{pi}} \sigma_{pi} \cdot d\epsilon_{pi}}{\sum_{k=1}^n \int_{\epsilon_{p(k-1)}}^{\epsilon_{pk}} \sigma_{pk} \cdot d\epsilon_{pk}} \quad (30)$$

Where i and k are the cycle numbers; n is the cycle number at concrete failure; σ_{pi} is the applied compressive stress during (PHC)_i; $d\epsilon_{pi}$ is the differential strain during (PHC)_i; and $\int_{\epsilon_{p(i-1)}}^{\epsilon_{pi}} \sigma_{pi} \cdot d\epsilon_{pi}$ is the area under the curve of stress-strain during (PHC)_i which is

abbreviated as (PHCSSA)_i.

To apply this damage index, the stress-strain data of the finite element is needed.

Fig. 15 compares the proposed microscopic damage index, calculated for concrete confined within rectangular transverse reinforcements with a spacing of 6 cm and a diameter of 9 mm with unconfined concrete of strength of $f'_c = 35$ MPa under cyclic loading.

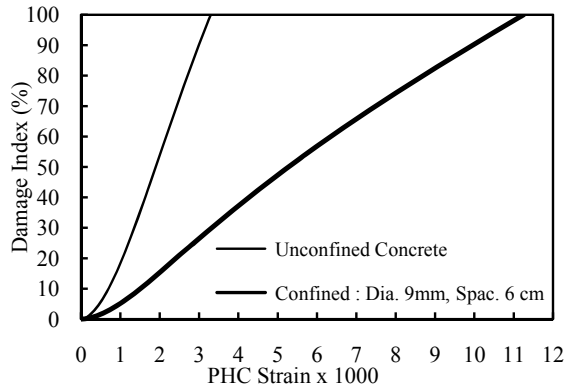


Fig. 15 Microscopic damage index, calculated for confined and unconfined concretes under cyclic loading

5.3. Proposition of a simplified macroscopic damage index for RC structural members

Based on the evidence that the structural member is highly affected in the critical zone (section), the main bending effect is due to the curvature registered at critical sections. Actually after the peak value on the response curve of critical section, very significant local effects occur at the critical section where a pseudo plastic hinge appears. Once the peak has passed, curvature enhancement is concentrated at the critical zone (section), while in the other regions, the curvatures decrease rapidly to near zero and cracks openings are closed. To determine force-displacement relationships for different sections of a structural member to apply the global energy-based damage index (D) requires a very time consuming calculation of the structural member's displacement. Further, the structural member response is highly affected in the critical zone (section), a comparable simplified moment-curvature based macroscopic damage index (D), derived from the global energy-based damage index proposed by the author [4] as represented by the equations (31), (32) and (33) is proposed in this paper.

$$D = \text{Max} [D^+, D^-] \quad (31)$$

$$D^+ = \frac{\sum_{i=1}^{i=n} \int_{\varphi_{p(i-1)}}^{\varphi_{pi}} M_{pi}^+ \cdot d\varphi_{pi}^+}{\sum_{k=1}^{k=n} \int_{\varphi_{p(k-1)}}^{\varphi_{pk}} M_{pk}^+ \cdot d\varphi_{pk}^+} \quad (\text{for} \quad (32)$$

PHC positive curvatures)

$$D^- = \frac{\sum_{i=1}^{i=n} \int_{\varphi_{p(i-1)}}^{\varphi_{pi}} M_{pi}^- \cdot d\varphi_{pi}^-}{\sum_{k=1}^{k=n} \int_{\varphi_{p(k-1)}}^{\varphi_{pk}} M_{pk}^- \cdot d\varphi_{pk}^-} \quad (\text{for} \quad (33)$$

PHC negative curvatures)

Where i and k are the cycle numbers; n is the cycle number at structural member's failure; M_{pi}^+ and M_{pi}^- are the applied bending moments during (PHC)_i⁺ and (PHC)_i⁻ in positive and negative directions, respectively; $d\varphi_{pi}^+$ and $d\varphi_{pi}^-$ are the differential curvature during (PHC)_i⁺ and (PHC)_i⁻ for positive and negative PHC curvatures, respectively; $\int_{\varphi_{p(i-1)}}^{\varphi_{pi}} M_{pi}^+ \cdot d\varphi_{pi}^+$ and $\int_{\varphi_{p(i-1)}}^{\varphi_{pi}} M_{pi}^- \cdot d\varphi_{pi}^-$ are the area under the curve of moment-curvature during (PHC)_i⁺ and (PHC)_i⁻ in positive and negative directions which are abbreviated as (PHCMCA)_i⁺ and (PHCMCA)_i⁻, respectively.

The evaluation of the (PHCMCA)_i⁺, (PHCMCA)_i⁻ and "D" is illustrated by the example shown schematically in Fig. 16 for cyclic loading. Fig. 16 shows a typical moment-curvature curve for critical section of a RC column under cyclic loading. The (PHCMCA)₁⁺ of the first PHC corresponds to the area under the curve of OAA'.

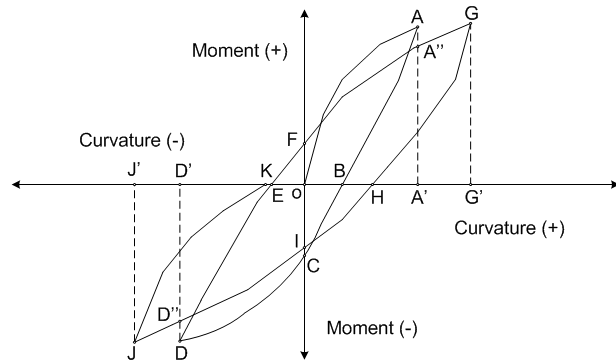


Fig. 16 Schematic illustration of damage index "D" calculation procedure for cyclic loading

During unloading towards point B, the "D" retains its value. Following the loading cycle to the point C, is a "following half-cycle" in positive direction. "D" is still zero. The change in sign of (PHCMCA)_i⁺ occurs at the points of symmetry about the origin of the coordinate system. For the first PHC in the negative curvature range, (PHCMCA)₁⁻ is equal to the area under the curve OCDD'. The recovered moment-curvature area between points D and E is not considered, and "D" retains its value. Loading between points E and F is the first FHC in the negative direction. Further loading in the positive direction up to point A" (maximum positive curvature to date) is equal to a new FHC. After point A", a new PHC for positive curvatures is formed. (PHCMCA)₂⁺ is equal to the area under the curve A''GG'A'. Subsequent cycles are analyzed with the same procedure and the damage index "D" is calculated.

In Fig. 17, the macroscopic "D" calculated for two columns under cyclic and monotonic loading versus top horizontal displacement are shown.

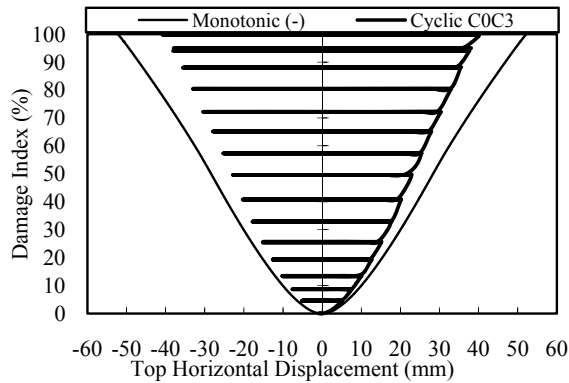


Fig. 17 Macrospecific Damage index, calculated for tested columns under cyclic and monotonic loading

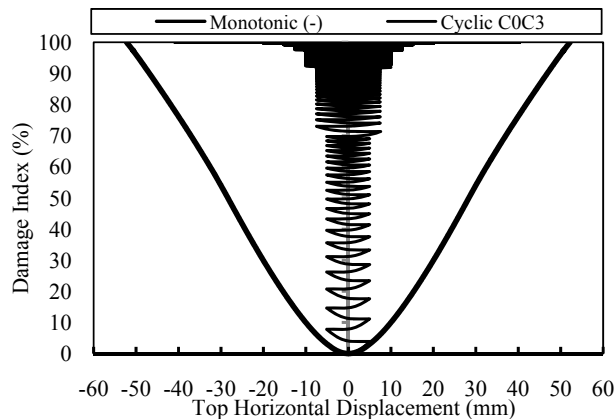


Fig. 18 Meyer's Damage index, calculated for tested columns under cyclic and monotonic loading

In Figs. 17 and 18, the proposed and Meyer's indices calculated for columns C0C3 and C0M under cyclic and monotonic loading, versus top horizontal displacement are presented. As Fig. 17 indicates, this column under cyclic loading is damaged only during positive displacements; therefore the increasing of "D" is mainly due to "D⁺". Some other tested columns are damaged during both positive and negative displacements, and the increasing of "D" for these is due to both "D⁺" and "D⁻".

Comparing the values given in Figs. 17 and 18 with damage phases shows that the damage index proposed by Meyer is oversensitive to the number of cycles and is therefore, not applicable in case of loading comprising repeated cycles, while the proposed damage index provides a regular distribution adapted to different phases of damage up to failure for any type of loading. As an example, applying the column test results under cyclic loading with 20 repeated cycles per amplitude shows that Meyer's "D" reaches 71% in the phase of first tension crack appearance and 99.9% in the phase of first compression crack appearance, while in these phases the proposed "D" reaches 4.5% and 49.5%, respectively.

In monotonic loading cases, the proposed and Meyer's indices provide exactly the same results.

To calculate macrospecific "D", the moment-curvature data for the critical section is required. This data can be found from the numerical simulation of structures.

The comparison between values of the proposed damage index calculated based on experimental test data and numerical simulation results using SADEP for cyclic and monotonic loading cases shows that for the calculation of "D", performing expensive experimental tests is not necessary and using a nonlinear structural analytical simulation such as SADEP is sufficient.

The proposed damage indices are applicable for any type of cyclic and monotonic loading.

5.4. Damage phases

The microscopic damage index reaches between 50% and 60% at the peak point of the unconfined concrete's stress-strain curve and is between 20% and 25% at the peak point of the confined concrete stress-strain curve. It reaches 100% at failure.

For the tested RC columns under cyclic lateral oriented loading and axial loading, the values of the proposed macrospecific damage index, reached about 5% in the phase of the first tensile cracks appearance, between 45% to 50% when the first compression cracks occurred, and 100% at failure.

6. Conclusions

The proposed stress-strain models for confined and unconfined concretes under the compression monotonic and cyclic loading is simple and applicable to simulate numerically the RC structure's behavior under monotonic and cyclic loading.

The proposed model is validated mainly by comparison with the results of experimental tests carried out on both concrete cylindrical samples and on RC full-scale columns subjected to cyclic mono-axial and biaxial bending moments with applied axial load performed by different researchers.

Since the proposed model has a strong mathematical structure, it can readily be adapted and achieve a higher degree of precision by modifying the relevant coefficients following the completion of more accurate and precise tests. The proposed model can be used in conjunction with finite element analysis for the simulation of a wide range of RC elements under any loading conditions.

The damage indices proposed in this paper are applicable to RC elements and structures subjected to cyclic and monotonic loading. They have been validated both by comparing the experimental data obtained in laboratory tests and nonlinear numerical simulation performed by SADEP. They are practical means for determining whether to repair or demolish structures after an earthquake. It can also be employed in the design of new structures as a design parameter to define the acceptable limit of damage as set by building codes.

Acknowledgements: The support of Ecole Central de Nantes/France, Water Resources Management Organization/Ministry of Energy/Iran and Girne American University/Cyprus are appreciated.

References

- [1] Sheikh SA, Uzumeri SM. Analytical model for concrete confined in tied columns, *Journal Structural Division*, ASCE, 1982, St. 12, Vol. 108, pp. 2703-2722.
- [2] Park YJ, Ang AHS. Mechanistic seismic damage model for reinforced concrete, *Journal of Structural Division*, ASCE, 1985, No. 4, Vol. 111, pp. 722-739.
- [3] Abbasnia R, Mirzadeh N, Kildashti K. Assessment of axial force effect on improved damage index of confined RC beam-column members, *International Journal of Civil Engineering*, 2011, No. 3, Vol. 9, pp. 237-246.
- [4] Sadeghi K. Energy based structural damage index based on nonlinear numerical simulation of structures subjected to oriented lateral cyclic loading, *International Journal of Civil Engineering*, 2011, No. 3, Vol. 9, pp. 155-164.
- [5] Garcia Gonzalez JJ. Contribution à l'étude des poteaux en béton armé soumis à un cisaillement dévié alterné, Thesis of Doctorate (PhD.), Ecole Central de Nantes, Nantes, 1990.
- [6] Park R, Kent DC, Sampson RA. Reinforced concrete members with cyclic loading, *Journal of the Structural Division*, Proceeding of the ASCE, 1972, ST7, pp. 1341-1359.
- [7] Sadeghi K. Numerical simulation and experimental test of compression confined and unconfined concretes, Technical report submitted to Water Resources Management Organization, Ministry of Energy, Concrete Laboratory of Power and Water University of Technology, Tehran, 2002.
- [8] Lamirault J. Contribution à l'étude du comportement des ossatures en béton armé sous cisaillement normales. Simulation par analyse non linéaire globale, Thesis of Doctorate (PhD.), Ecole Central de Nantes, Nantes, 1984.
- [9] Al Sulayfani B. Contribution à l'étude du comportement des ossatures en béton armé sous sollicitations cycliques par analyse non-linéaire globale, Thesis of Doctorate (PhD.), Ecole Central de Nantes, Nantes, 1986.
- [10] CEB, Confined concrete, CEB-FIP Model code 1990, Supplementary Documents for the first pre-draft, *Bulletin d'information*, 1988; No. 189.
- [11] Buyukozturk O, Shareef SS. Constitutive modeling of concrete in finite element analysis, *Journal of Computers & Structures*, 1985, No. 3, Vol. 21, pp. 581-610.
- [12] Meyer IF. Ein werkstoffgerechter schädigungsmodell und stababschnittselement für stahlbeton unter zyklischer nichtlinearer beanspruchung, 1988; SFB 151, Mitteilung No. 88-4.
- [13] Darwin D, Pecknold DA. Nonlinear biaxial law for concrete, *Journal of the Engineering Mechanics Division*, 1979, Vol. 105, pp. 623.
- [14] Bazant ZP, Kim SS. Plastic-fracturing theory for concrete, *Journal of Engineering Mechanics Division*, Proceedings of ASCE, 1979, EM3, Vol. 105, pp. 407-429.
- [15] Sinha BP, Gerstle KH, Tulin LG. Stress-strain relation for concrete under cyclic loading, *ACI Journal*, 1964, No. 2, Vol. 61, pp. 195-211.
- [16] Karsan ID, Jirsa JO. Behavior of concrete under compressive loading, *Journal of the Structural Division*, Proceedings of ASCE, 1969, ST12, Vol. 95, pp. 2543-2563.
- [17] Mander JB, Priestley MJN, Park R. Design of Bridge Piers, Report No. 84-2, Department of Civil Engineering, University of Canterbury, 1984.
- [18] Comité Euro-International du Béton, Code-Modèle CEB-FIP pour les structures en béton, *Bulletin d'information*, 1978, No. 124-125F, Vols. 1-2.
- [19] Sheikh SA. A comparative study of confinement models, *ACI Journal*, 1982, Vol. 296.
- [20] Sieffert JG, Lamirault J, Garcia Gonzalez JJ. Behavior of R/C columns under static compression and lateral cyclic displacement applied out of symmetrical planes, *Structural Dynamics*, Kratzig et al., Balkema, Rotterdam, 1990, Vol. 1.
- [21] Sadeghi K. Simulation numérique du comportement de poteaux en béton armé sous cisaillement dévié alterné, Thesis of Doctorate (PhD.), Ecole Central de Nantes, Nantes, 1995.
- [22] Abbasnia R, Holakoo A. An investigation of stress-strain behavior of FRP-confined concrete under cyclic compressive loading, *International Journal of Civil Engineering*, 2012, No. 3, Vol. 10, pp. 201-209.
- [23] Mander JB, Priestley MJN, Park R. Theoretical stress-strain model for confined concrete, *ASCE Journal*, 1984, No. 8, Vol. 114, pp. 1804-1826.
- [24] Belmouden Y, Lestuzzi P. Analytical model for predicting nonlinear reversed cyclic behavior of reinforced concrete structural walls, *Elsevier, Engineering Structures*, 2007, Vol. 29, pp. 1263-1276.
- [25] Otes A. Zur werkstoffgerechten Berechnung der Erdbebenbeanspruchung in Stahlbetontragwerken, *Mitteilungen aus dem Institut für Massivbau der TH Darmstadt*, 1985, Heft 25.